# Progressive Collapse Resistance of Precast Concrete Beam-Column Sub-assemblages with High-Performance Dry Connections

Kai Qian[1*], Shi-Lin Liang[1], Feng Fu[2], and Qin Fang[3]

[1] College of Civil Engineering and Architecture, Guangxi University, 100 Daxue Road, China, 530004.

[2] School of Mathematics, Computer Science and Engineering, Northampton Square, London, EC1V 0HB, U.K.

[3] Army Engineering University, Nanjing 210007, Jiangsu, Peoples R China

**Abstract:** Due to its relatively lower integrity, precast concrete structures are considered to be more vulnerable to progressive collapse than cast-in-place concrete structures. However, to date, majority of existing studies on progressive collapse focused on cast-in-place concrete structures, little attentions were paid to precast concrete structures. Among existing precast concrete structures, unbonded post-tensioning precast concrete structure is one of innovation dry connection structural systems, which no casting at the connections on site. Its excellent seismic performance was recognized by many studies, while studies on its progressive collapse resistance were very few. To fill this knowledge gaps, in this paper, eight half-scaled unbonded post-tensioning precast concrete beam-column sub-assemblages with different connection configurations were tested through pushdown tests to investigate their capacities and resistance mechanisms to prevent progressive collapse. The test results demonstrated various behaviors of beam-column sub-assemblages with different connection types. It was found that, as the longitudinal reinforcements were discontinuous across the beam-column joint region in the beams, flexural action observed in the cast-in-place concrete frames was not mobilized for the specimens with purely unbonded post-tensioning connections. When the specimens installed top-seat angles at the beam-column interfaces, considerable flexural action capacity could be mobilized for load resistance. Moreover, it was found that the failure modes of the specimens are distinctly different to that of conventional reinforced concrete frames or precast concrete frames with cast-in-place joints. The characteristic of compressive arch action and tensile catenary action in tested specimens is quite different to that of conventional reinforced concrete frames.

* Corresponding author. E-mail address: qiankai@gxu.edu.cn

## 1. Introduction

Due to the advantages of environment friendly, fast track construction, large bulk of offsite production, and high-quality workmanships, precast concrete (PC) structures are widely used in the construction projects worldwide. However, as the beam longitudinal reinforcements are discontinuous in the beam-column joint, PC frames with normal dry connections are more vulnerable to progressive collapse, compared to conventional cast-in-place reinforced concrete (RC) frames. To date, majority of attentions were paid on monolithic cast-in-place RC structures to resist progressive collapse. Su et al. [1] tested twelve 1/2 scaled specimens to investigate the effects of beam reinforcement ratio, span-to-depth ratio, and loading rate on compressive arch action (CAA) capacity of RC beam-column sub-assemblage. Sadek et al. [2] tested two full-scale RC sub-assemblages with different seismic details. Yu and Tan [3] experimentally investigated the effects of seismic design on the performance of RC frames in mitigating progressive collapse. Yu and Tan [4] proposed three special detailing to enhance the progressive collapse resistance of RC frames. Ren et al. [5] and Lu et al. [6] carried out a series of tests on beam-slab and beam-column sub-assemblages subjected to edge or middle column missing scenario to investigate the contribution of RC slabs in progressive collapse resistance. Qian et al. [7] discussed the contribution of each alternate load path of RC buildings, such as CAA, tensile catenary action (TCA), and compressive/tensile membrane action to resist progressive collapse. Qian and Li [8-9] filled knowledge gaps for RC frames subjected to the loss of a corner column. Meanwhile, the benefits from slab to resist progressive collapse were quantified by Qian and Li [10-11]. It was found that the RC slab could significantly improve the behavior of RC buildings against progressive collapse. Shan et al. [12] tested two 1/3 scale, four-bay by two-story RC planar frames to investigate the effects of infilled wall on the load resisting mechanisms of RC frames. It was found that the infill walls could enhance the load resisting capacity of frames significantly. Peng et al. [13-14] experimentally evaluated the dynamic response of flat plate structure subjected to an exterior or interior column removal scenario. Ma et al. [15] tested a 1/3 scaled RC flat plate substructure to assess its behavior under a corner column removal scenario. Qian et al. [16] investigated the advantages of using steel braces to strengthen the progressive collapse resistance of RC frames. The steel brace increased the initial stiffness and CAA capacity significantly whereas few benefits for TCA were observed, due to compressive buckling or tensile fracture in braces at large displacement stage. Sasani et al. [17-21] conducted a series of on-site tests to capture the behavior of RC multi-storey structure subjected to different initial damages. These on-site tests evaluated the load resisting contribution from Vierendeel action, flexural action, and non-structural element such as infill walls. However, studies on PC frames to resist progressive collapse were very few. Nimse et al. [22] studied the progressive collapse behavior of PC beam-column sub-assemblages with monolithic joints. Kang and Tan [23] experimentally investigated the effects of joint reinforcement detailing and reinforcement ratio on load resistance of PC beam-column sub-assemblages. Kang and Tan [24] test four specimens to assess the robustness of PC frames subjected to the loss of a penultimate column scenario. It was found that, with reasonable anchorage details, the PC structures with cast-in-place topping could obtain similar behavior as RC structures. Keyvani [25-26] conducted studies on behavior of precast prestressed concrete flat slab floor to resist progressive collapse. It was found that bonded post-tensioned floor system was more susceptible to failure after column removal than unbonded one due to localization of tendon strains. Qian and Li [27] tested two large-size PC and beam-column-slab substructures with monolithic joints and one reference RC substructure to investigate the load resisting mechanism of PC frames. It was indicated that CAA, TCA could be developed in PC beams and compressive/tensile membrane actions could be developed in PC hollow core slabs with cast-in-place topping layer. However, it should be noted that PC construction with cast-in-place monolithic joints (wet joints) could not reflect the advantage of PC construction sufficiently. Therefore, the performance of PC frames with dry connections to mitigate progressive collapse was investigated by Al-Salloum et al. [28], Quiel et al. [29], and Qian and Li [30]. These tests indicated that PC frames with welded connection could not develop TCA owing to the early failure of the welded connection. The PC frames with bolted connection could not develop

CAA in PC beams as the gap between the beam and column allows the PC beams to expand outward. The bolted connection could prevent the PC beams to develop TCA, as the reinforcements were discontinuous at the beam-column joints.

From above existing studies, it can be seen that, it is imperative to evaluate the robustness of PC frames with other types of dry connections to resist progressive collapse. PC frames with unbonded post-tensioning (UPT) strands were one of innovative dry connections, which was initially proposed by PREcast Seismic Structural System (PRESSS) program. A number of tests [31-32] had been carried out for the evaluation of the seismic behavior of PC frames with UPT strands. It was found that the PC frames with UPT strands could provide desirable load carrying and deformation capacity with little residual damage. However, the PC frame with UPT strands has low energy dissipation capacity. Therefore, to enhance the energy dissipation capacity of the system, several studies were conducted. Santon et al. [33] and stone et al. [34] placed extra mild rebar grouted in ducts in the beam-column joints regions to dissipate extra energy (hybrid system). It was found that the load resistance and energy dissipation capacity of the hybrid systems can match that of cast-in-place RC system. Then, Rodgers et al. [35-36] proposed new energy dissipation devices for hybrid system. Song et al. [37-38] conducted a series of tests on a novel hybrid connection. In such a connection, steel jackets were installed at the beam ends to achieve damage avoidance. The test results revealed favorable reparability in addition to self-centering and energy dissipation capacity of the novel connection. However, the aforementioned studies were mainly focused on the performance of the PC system with UPT strands or hybrid system subjected to cyclic load. Few studies were carried out to investigate their resistance to progressive collapse (monotonic load). Therefore, in this paper, a series of eight one-half scaled PC beam-column substructures with three different types of connections (UPT connection, hybrid connection with additional bolted top-seat angle, and pure bolted top-seat angle connection for comparison purpose) were tested under quasi-static pushdown loading regime.

## 2. Experimental program

Fig. 1 shows the difference of bending moment diagram of a frame before and after removal of a column (interior or penultimate column). It can be seen that, the bending moment in the middle joints above the removed column changed from negative to positive after removal, whereas the negative bending moment at the side joints increased significantly. As this is overlooked in conventional structural design, the structures may suffer severe damage and worth investigating their load redistribution abilities. For this purpose, beam-column sub-assemblages were extracted from the frame at the points of contra-flexure, as shown in Fig. 1b. As shown in the figure, the sub-assemblages subjected to the loss of an interior column (called interior sub-assemblage) or a penultimate exterior column (called exterior sub-assemblage) were investigated for the evaluation of the influence of horizontal constraints on the behavior of PC beam-column sub-assemblages in resisting progressive collapse. The main difference between interior and exterior sub-assemblages was the degree of horizontal constraints at the side columns.

### *2.1. Test specimens*

The prototype building is an eight-storey frame, which was designed in accordance with ACI 318-14 [39]. The prototype frame was located on a D class site. The design spectral response acceleration parameters of SDS and SD1 are 0.46 and 0.29, respectively. The design live load of the prototype frame is 2.0 kPa. The dead load including the ceiling weight is 5.1 kPa. Fig. 2 shows the configuration of three different connections: a) UPT connection, b) hybrid connection with additional top-seat angles, c) connected solely by top-seat angles for comparison purpose. Table 1 tabulates the relationship between prototype frame and test specimens, while Table 2 summarized main characteristics of the test specimens. As listed in the Table 2, eight half-scaled specimens, which can be categorized into three groups (UP, TSUP, and TS), were tested. The design variables are connection types, effective prestressing force in strands, and locations of the lost column. UP, TSUP, and TS represent unbounded post-tensioning connection, hybrid connection, and top-seat angle connection, respectively. The letter E and I denote exterior and interior sub-assemblages, respectively. The last numeral denotes effective prestress in unbonded strands. Thus, TSUPE-0.4 indicates an exterior sub-assemblage with effective prestress of $0.4f_{pu,}$ which was assembled by hybrid connection, where $f_{pu}$ denotes nominal ultimate strength of the post-tensioning strands (1860 MPa herein). Due to symmetry, only half of the specimen was exhibited in Fig. 3. It should be noted that all specimens have identical cross section of beam and column as well as reinforcement details (refer to Table 1). The nominal diameter and area of unbonded strand are 12.7 mm and 97.8 $mm^2$, respectively. The beam longitudinal rebar of 2T12 was placed at both top and bottom layers, which were discontinuous at the joint. 4T16 were used as column longitudinal reinforcement. R6 were used as transverse reinforcement. T12 and T16 denote deformed bars with diameter of 12 mm and 16 mm, respectively, while R6 indicates plain rebar with diameter of 6 mm.

### *2.2. Material properties*

The concrete used to cast UPE-0.4, UPI-0.4, and UPI-0.65 had an average cylindrical compressive strength of 40.0 MPa and a tensile splitting strength of 3.7 MPa. For the rest of specimens, the cylindrical compressive strength and tensile splitting strength were 38.5 MPa and 3.5 MPa, respectively. The material used for top-seat angle was Grade S235, whereas Grade 8.8 M18 bolts was employed to fix the top-seat angles with torque of 215 N·m. The properties of rebar and post-tensioning strand were shown in Table 3 and Fig. 4.

### *2.3. Pushdown test setup*

The experimental setup is shown in Fig. 5. The side column bottoms were anchored to the pin supports via four high-strength bolts, and then the pin supports were fixed to the strong floor by high strength bolts with diameter of 50 mm. Each overhanging beam was connected to the A-frames through a roller. Moreover, the top of side column was bolted with a steel extension that connected to the A-frame via an additional roller. A self-equilibrium system was employed to apply an axial compressive force at the side column. A hydraulic jack (Item 1 in Fig. 5a) beneath the H-frame was used to apply vertical displacement. In order to eliminate possible out-of-plane failure of the specimens, a steel assembly (Item 3 in Fig. 5a) was specially designed to provide out-of-plane restraints to the specimens.

### *2.4. Instrumentation*

To monitor the structural response accurately, extensive instrumentation was installed to monitor test results. The horizontal reaction forces from column top and overhanging beam were measured by two tension /compression load cells (Item 5 in Fig. 5a), which were installed at the roller. However, a load pin (Item 8 in Fig. 5a), which was installed at the bottom support, was used to measure the horizontal and vertical reaction forces at the pin support. The applied vertical load was captured by a load cell (Item 2 in Fig. 5a) installed beneath the hydraulic jack. Meanwhile, two load cells (Item 7 in Fig. 5a) were installed at jacking end of the strands to monitor the variation of prestressing forces during tests. As shown in Fig. 5b, the overall vertical deflection of the beam and lateral movements of the side column were measured by a series of linear variable differential transformers (LVDTs). Moreover, strain gauges were amounted onto the reinforcements symmetrically before casting.

## 3. Test results

Eight specimens were tested through pushdown loading regime. The critical test results, for instance, the first peak load (FPL), ultimate load (UL), and the maximum horizontal compressive or tensile forces were summarized in Table 4. Fig. 6 illustrates the relationship of applied load versus middle joint displacement (MJD) of tested specimens. More detail description and discussion could be found in following sections.

### *3.1. Global behavior and failure modes*

***Specimens with bolted top-seat angle connection***

TSE and TSI have identical dimensions and reinforcement details except different boundary conditions. The axial compressive force ratio of 0.2 was applied at the side column. Compared to TSE, TSI has overhanging beam beyond the side column. It can be observed from Fig. 6 that TSI and TSE obtained UL of 12.1 kN and 11.6 kN at MJD of 100 mm and 60 mm, respectively. The applied load began to decrease gradually until the end of test. The test results indicated the TCA resistance of TSE and TSI is negligible, as the beam reinforcements were discontinuity and the top-seat angle unable to provide sufficient tie-force.

The failure modes of TSE and TSI were shown in Figs. 7 and 8, respectively. The beam and column almost detached completely at large deformation stage. For TSE, the failure was concentrated at the beam ends and only a few thin flexural cracks observed at the beam and side column. For TSI, it was quite similar to that of TSE except no crack formed at the side columns. This is because the overhanging beam restricted the deformation of the side columns effectively. It is worth noting that the top-seat angles experienced limited deformation.

***Specimens with unbonded post-tensioning connection***

UPE-0.4 has effective prestress of $0.4f_{pu}$ in unbonded strand and the axial compressive force ratio of the side column is 0.2. The FPL of UPE-0.4 was measured to be 30 kN at an MJD of 45 mm, whereas the UL was measured to be 73 kN when the MJD up to 540 mm. Finally, test was stopped due to excessive horizontal deflection in the right-hand side column. Fig. 9 shows the failure mode of UPE-0.4. As shown in the figure, the failure mode of UPE was quite different to that of TSE and TSI. Concrete crushing occurred at the compressive toes of the PC beam rather than concrete spalling occurred at the beam end. No cracks occurred along the beam whereas wide opening was found at beam-column interface due to fixed-end rotation. Moreover, due to tensile force from strands and axial compression at the side column, a typical large eccentric compressive failure was observed at the right-hand side column, which resulted in extensive flexural cracks occurred at the inner side of the column, but severe concrete crushing occurred at the outer side. However, the left-hand side column experienced much milder damage, only several thin flexural cracks formed in the inner side. The different failure mode of two side columns was because the damage always occurs in relatively weak side first and then concentrated in this side in the latter loading steps.

UPI-0.4 has overhanging beam at both sides. For UPI-0.4, the FPL of 35 kN was measured at an MJD of 29 mm. Thus, the FPL of UPI-0.4 was approximately 116.6 % of that of UPE-0.4. With the increase of MJD, the opening at the beam-column interfaces became wider and wider. Meanwhile, the concrete crushing in the compressive toes of the beam end became more severe. When the MJD reached 631 mm, one wire of the bottom strand fractured, as a result, the applied load dropped from 150 kN to 142 kN. Afterwards, the applied load kept increasing until the end of test. The UL of UPI-

0.4 was 151 kN at an MJD of 652 mm, which was approximately 206.8 % of that of UPE-0.4. As shown in Fig. 10, the failure mode of UPI-0.4 was quite different to that of UPE-0.4. Wide opening was observed at the beam-middle column interface and complete detach was observed between the beam and side column surfaces. Thus, the progressive collapse resistance was totally provided by two unbonded strands in large deformation stage. Moreover, due to considerable horizontal stiffness provided by overhanging beam, the damage of the side column of UPI-0.4 was less severe and only thin flexural cracks occurred along the side columns.

UPI-0.65 has similar dimensions and reinforcement details as UPI-0.4 except higher effective prestress of $0.65f_{pu}$ was applied. When the MJD reached 39 mm, the FPL of 44 kN was measured, which was 125.7 % of that of UPI-0.4. Thus, the specimen with higher effective prestress would obtain higher resistance at small deformation stage. When the MJD reached 542 mm, the UL of 131 kN, which was 86.8 % of that of UPI-0.4, was measured. After that, fracture of the wires of the strands was observed consecutively until both two unbonded strands fractured completely at an MJD of 628 mm. As shown in Fig. 11, except the fracture of both strands, the failure mode of UPI-0.65 was quite similar to that of UPI-0.4.

***Specimens with hybrid connection***

TSUPE-0.4, TSUPI-0.4, and TSUPI-0.65 were, respectively, have the enhancement over UPE-0.4, UPI-0.4, and UPI-0.65 through extra bolted top-seat angle installed at the beam-column interface. The FPL and UL of TSUPE-0.4 were 49 kN and 83 kN at MJD of 80 mm and 522 mm, respectively, which were 163.3 % and 113.7 % of that of UPE-0.4, respectively. Thus, the bolted top-seat angle enhanced the load resistance effectively, especially for the FPL at relatively small deformation stage. Fig. 12 shows the failure mode of TSUPE-0.4. As shown in the figure, severe concrete spalling occurred at the beam end and cracks formed at the beam end and side column. Moreover, concrete crushing was observed at outer sider of the side columns. In general, the failure mode of TSUPE-0.4 was almost a combination of that of TSE and UPE-0.4 except top-seat angles achieved larger deformation.

Compared to TSUPE-0.4, TSUPI-0.4 has overhanging beam beyond the side column. When MJD reached 95 mm, the FPL of 51 kN, which is about 145.7 % of that of UPI-0.4, was measured. Similar to TSUPE-0.4, severe flexural cracks were observed at the beam ends when the MJD reached 250 mm (about one beam depth). With increasing MJD to 330 mm, flexural crack was first observed in the left side column. Test was stopped when the displacement reached 600 mm with a UL of 181 kN, which was approximately 119.9 % of that of UPI-0.4. As shown in Fig. 13, in general, the failure mode of TSUPI-0.4 was quite similar to that of TSUPE-0.4 except TSUPI-0.4 experienced much milder damage in side columns.

With a higher effective prestress of $0.65f_{pu}$, TSUPI-0.65 obtained a higher FPL of 64 kN at an MJD of 76 mm. The UL of 178 kN was measured at an MJD of 600 mm. When the MJD reached 290 mm, the flexural cracks were first observed in the left side column, which were earlier than that of TSUPI-0.4. As shown in Fig. 14, in general, the failure mode of TSUPI-0.65 was quite similar to that of TSUPI-0.4. It was noted that the top-seat angles of TSUPI-0.65 experienced larger deformation than that of TSUPI-0.4.

### *3.2. Horizontal reaction*

Fig. 15 shows the comparison of total horizontal reaction versus MJD curves of tested specimens while Table 4 tabulated the maximum horizontal reaction force. As shown in the figure and Table 4, the maximum horizontal compressive force in UPE-0.4, UPI-0.4, UPI-0.65, TSUPE-0.4, TSUPI-0.4, and TSUPI-0.65 were -66 kN, -96 kN, -84 kN, -50 kN, -93 kN, and -113 kN, respectively. Therefore, UPE and TSUPE obtained much lower horizontal compressive force compared to the counterpart UPI and TSUPI specimens due to no overhanding beams providing additional constraints. In addition, the maximum tensile force of UPE-0.4, UPI-0.4, UPI-0.65, TSUPE-0.4, TSUPI-0.4, and TSUPI-0.65 were 139 kN, 323 kN, 321 kN, 146 kN, 380 kN, and 364 kN, respectively. Comparison of the maximum horizontal tensile force shows that UPE and TSUPE only achieved half of the maximum horizontal tensile force as that of UPI and TSUPI specimens.

Fig. 16 illustrates the decomposition of the contribution of horizontal reaction force of UPI-0.4 and UPE-0.4. As shown in Fig. 16a, for UPI-0.4, bottom pin provided the largest contribution for the compressive force while the overhanging beam provide the largest portion of the tensile force. For specimen UPE-0.4, as no overhanging beams beyond the side column, the bottom pin and column top roller provide almost similar contribution in tensile force. However, similar to UPI-0.4, majority of the compressive force was contributed by the pin beneath the side column.

### *3.3. Deflection*

Fig. 17a illustrates the overall deflection of the beams of UPI-0.65. As plastic hinges did not form at the beam ends during the test, the beam elements deformed straightly. In general, the beams in the specimens with UPT connection deformed straightly. Fig. 17b shows the deformation shape of TSUPI-0.65. Different to UPI-0.65, TSUPI-0.65 was deformed in double curvature manner, which agreed well with the observations that flexural action was mobilized at the beam end to resisted load. Similar phenomena were observed for other specimens with hybrid connections. Figs. 18a and b show the lateral deflection of the left side column of TSUPE-0.4 and TSUPI-0.4, respectively. As shown in the figure, the side columns were pushed outward (negative value) firstly due to compressive axial force developed in the beams. In large deformation stage, they were pulled inward (positive value) because considerable tensile force developed in the strands. The measured maximum inward movement in TSUPE-0.4 and TSUPI-0.4 were 24.2 mm and 6.2 mm, respectively. Compared to TSUPE-0.4, due to desirable horizontal constraint provided by overhanging beams, the side column of TSUPI-0.4 experienced less lateral deflection. In general, all the exterior side columns (without overhanging beam) suffered a much larger deformation than interior ones (with overhanging beam).

### *3.4. Strain gauge results*

The strain distributions along beam longitudinal reinforcements of UPE-0.4, UPI-0.4, and TSUPI-0.4 were demonstrated in Figs. 19, 20, and 21, respectively. As shown in the figure, compressive strain about -180 με was initially measured due to the effects of effective prestress of

$0.4f_{pu}$ in post-tensioning strands. As shown in Fig. 19a, the strain of the bottom reinforcement near the middle joint reduced to 0 με when an MJD reached 20 mm, which could be explained as the opening formed in the bottom of the beam end near the middle column. However, the strain of the bottom reinforcement near the side column kept increasing with further increasing the MJD due to the rotation of the beam end near the side column compacted the bottom of the beam section more tightly. Conversely, due to similar reasons, for top reinforcements, the beam reinforcement near the middle joint kept increasing with increase of the MJD while the beam reinforcement near the side column decreased to 0 με soon. As shown in Fig. 20, the varying of strain in beam longitudinal reinforcement of UPI-0.4 was very similar to that of UPE-0.4. However, as illustrated in Fig. 21, the strain gauge results in beam longitudinal reinforcements of TSUPI-0.4 were quite different. As shown in Fig. 21a, for bottom reinforcements, tensile strain was measured at the beam end near the middle joint when the MJD less than 250 mm. After MJD beyond 250 mm, the tensile strain began to decrease as the top-seat angle began to quit work and wide opening occurred at the beam-middle column interface. For the strain in the bottom reinforcement near the side column, compressive strain of -2281 με was measured at an MJD of 100 mm. After that, the compressive strain began to decrease as severe concrete crushing in the beam end. For the top reinforcement, the overall trend was similar to that of the bottom rebar, whereas the maximum tensile and compressive strain, respectively, was measured to be 1886 με and -2278 με when the displacement up to 100 mm.

### *3.5. Prestressing forces*

Fig. 22 shows the variation of total prestressing forces in unbonded strands. The initial effective prestressing force in UPE-0.4, TSUPE-0.4, UPI-0.4, TSUPI-0.4, UPI-0.65, and TSUPI-0.65 were 153 kN, 148 kN, 150 kN, 146 kN, 237 kN, and 242 kN, respectively. In addition, the measured maximum prestressing force in UPE-0.4, TSUPE-0.4, UPI-0.4, TSUPI-0.4, UPI-0.65, and TSUPI-0.65 were 269 kN, 277 kN, 323 kN, 364 kN, 329 kN, and 368 kN, respectively. Therefore, all the strands in the specimens with overhanging beam reached their yield strength, which indicates the stronger boundary better explores the full capacity of the prestress strands. Furthermore, it was found that the prestressing forces in specimens with hybrid connections developed faster than others. This is because, for a given MJD, the elongation of strands in these specimens was larger than others. It should be noted that the strands in UPI series specimens fractured earlier than that in TSUPI series specimens. This maybe because UPI series specimens concentrated the main rotation at the beam-column interfaces (opening) whereas TSUPI series specimens deformed in a double-curvature manner and the most critical section was at the edge of the top-seat angle plate, which resulted in the stress distribution in the strands of TSUPI series more uniform.

## 4. Discussions of the test results

### *4.1. Effects of boundary conditions*

As listed in Table 4, the FPL of UPE-0.4 and UPI-0.4 were 30 kN and 35 kN, respectively. In addition, the UL of UPE-0.4 and UPI-0.4 were measured to be 73 kN and 151 kN, respectively. Therefore, for specimens with UPT connections, stronger horizontal restraints could enhance the FPL and UL by 16.7 % and 106.8 %, respectively. Furthermore, compared to UPI-0.4, UPE-0.4 achieved less tensile force in strands, which could be explained to the large eccentric compression failure in the side columns without overhanding beams. Regarding the failure modes, due to the additional horizontal constraints of overhanging beam, the side columns of UPI-0.4 experienced much milder damage, compared to UPE-0.4. For specimens with hybrid connection, the FPL of TSUPE-0.4 and TSUPI-0.4 were 49 kN and 51 kN, respectively. Thus, the overhanging beams had little effects on the PFL of the specimens with hybrid connections. When the MJD up to 600 mm and 522 mm, the UL of TSUPI-0.4 and TSUPE-0.4 were measured to be 181 kN and 83 kN, respectively. Thus, due to the overhanging beams, the TSUPI-0.4 increased UL by 118.1%, compared to TSUPE-0.4.

### *4.2. Effect of effective prestress force*

As listed in Table 4. The FPL of UPI-0.4, UPI-0.65, TSUPI-0.4, and TSUPI-0.65 were 35 kN, 44 kN, 51 kN, and 64 kN, respectively. Thus, the higher effective prestress in post-tensioning strands could increase the FPL of UPI and TSUPI series by 25.7 % and 27.5 %, respectively. As shown in Fig. 6, the growth of load resistance of UPI-0.65 and TSUPI-0.65 were slower than that of UPI-0.4

and TSUPI-0.4 at the beginning of the test. This is mainly due to the higher effective prestress force may result in the strands reach their yield strength earlier. Moreover, the fracture of strand was firstly observed in UPI-0.65 at an MJD of 542 mm while it was 621 mm for UPI-0.4. Thus, the higher effective prestress may lead to earlier fracture of the strands and reduce its deformation capacity. Therefore, in general, lower effective (less than 0.65 $f_{pu}$) prestress was preferred for post-tensioned precast concrete frame to resist progressive collapse, similar to Cheok and Lew [40] for seismic resisting design.

### *4.3. Effect of top-seat angle*

Compared to UPI-0.4, TSUPI-0.4 increased the FPL and UL by 45.7 % and 19.9 %, respectively. Thus, installing top-seat angle could improve the collapse resistance effectively. Moreover, due to the rotation restraint provided by the top-seat angle, the failure mode TSUPI-0.4 was significantly different to that of UPI-0.4. For UPI-0.4, wide opening was observed at the beam-column interface and no crack occurred along the beam. For TSUPI-0.4, severe flexural cracks were observed in the beams. Similar results were observed in TSUPE-0.4 and TSUPI-0.65. In general, installing top-seat angle could enhance the load resistance significantly and the flexural action could be mobilized to resist progressive collapse.

Fig. 23a compares the load resistance of TSUPI-0.4 to the superposition of TSI and UPI-0.4. As shown in the figure, the resistance of TSUPI-0.4 was larger than the superposition of TSI and UPI-0.4 from the beginning to the end. Thus, the hybrid connection achieved better resistance than the overall resistance capacity of two separate connections effect of one plus one over two. This is because the top-seat angle evoked flexural action and reduced the effective length of beam. In general, similar observations were obtained for TSUPE-0.4 and TSUPI-0.65, as shown in Fig. 23b and c.

### *4.4. Dynamic load resistance*

Based on the energy balance method proposed by Izzuddin [41], the external work is equal to the strain energy increased in the remained structure. Thus, the quasi-static progressive collapse resistance can be converted to dynamic resistance, that is, pseudo-static progressive collapse resistance. The dynamic progressive resistance can be determined by equation below:

$$P_{CC}(u_d) = \frac{1}{u_d}\int_0^{u_d} P_{NS}(u)du \qquad (1)$$

where $P_{CC}(u)$ and $P_{NS}(u)$ represent the capacity function and the nonlinear static loading estimated at the displacement demand $u$, respectively.

Fig. 24 illustrates the dynamic load resistance of the tested specimens. The dynamic load resistance of UPE-0.4, UPI-0.4, UPI-0.65, TSUPE-0.4, TSUPI-0.4, and TSUPI-0.65 were 49 kN, 71 kN, 67 kN, 62 kN, 89 kN and 91 kN, respectively. As shown in the figure, installing top-seat angles could enhance the dynamic load resistance up by 35.8 %.

### *4.5. Load resisting mechanisms*

Typical load resisting mechanisms of conventional RC frame are demonstrated in Fig. 25. As shown in Fig. 25a, flexural action and CAA were mobilized in sequence to resist progressive collapse at relatively small deformation stage. Flexural action depends on the bending moment capacity of the plastic hinge whereas CAA relies on the horizontal constraints at the beam ends. In general, with the increase of the MJD, the concrete crushing may lead to the termination of CAA. When the MJD exceeds about one beam depth, as shown in Fig. 25b, the axial force in the beam may change from compression to tension and TCA was mobilized to resist load. For RC structures, the decreasing of TCA was usually accompanied by rebar fracture. Moreover, penetrate cracks usually occur along the beam due to tensile axial force.

However, the load resisting mechanisms developed in PC frames observed in this study were quite different to that of conventional RC frames, as shown in Fig. 26. For specimens with UPT connection, as no beam longitudinal rebar passed through the beam-column joint, plastic hinge would not form at the beam end and thus, flexural action was not mobilized to resist the load. From the beginning of the test, the CAA and the tensile force developed in the strands together to resist the load. However, different to RC frames, the CAA mobilized in beam will not be terminated as the compressive force was actively applied by prestressing strands. Thus, the CAA may have a negative contribution to the load resistance when the displacement beyond about one beam depth. As shown in Fig. 26a, when the displacement was small, the arching force (N in the figure) developed in beams started to help to resist the vertical load (P in the figure). However, when the displacement exceeded about one beam depth, as shown in Fig. 26b, the direction of resultant force of the arching force would change from upward to downward, and thus, negative contribution generated. For specimens with UPT connections, as the CAA and TCA provided the load resistance independently. The contribution from TCA could be determined by the vertical component of prestressing forces. The contribution from CAA can be simply determined by subtracting the resistance of TCA from the measured load resistance. For the sake of brevity, only the decomposition of load resisting capacity of UPI-0.65 was shown in Fig. 27. As shown in the figure, the contribution of load resistance from TCA was always positive while the contribution of CAA will change from positive to negative when the vertical displacement beyond about one beam depth.

As shown in Fig. 28， for specimen with hybrid connection, flexural action was mobilized to resist progressive collapse as the top-seat angle constraints the rotation of beam end. It should be noted that, as the flexural action could not be simply determined. The decomposition of load resistance of specimens with hybrid connection was not shown herein. More detailed analysis should be carried out to determine the flexural action in the specimens with hybrid connection in the future study.

## 5. Conclusions

Based on the experimental results, the following conclusions can be drawn:

1. In RC structure, tensile catenary action (TCA) is kicked in after compressive arch action (CAA). However, in current study, the TCA in unbonded post-tensioning strands can be mobilized at the beginning of the test. Thus, the CAA and TCA can work simultaneously.
2. Different to RC frame, as no beam longitudinal reinforcements pass through the beam-column joint and the strands are unbonded, flexural action would not be developed to resist progressive collapse for the specimens with unbonded post-tensioning connection. However, flexural action

can develop in specimens with top-seat angle due to the top-seat angle constrains the rotation of beam end partially.

3. For conventional RC frame, CAA will be terminated when the vertical displacement beyond about one beam depth due to concrete crushing. However, in this study, the CAA developed in PC frames with unbonded post-tensioning strands was mainly due to prestressing force of the strands and thus, the CAA will not vanish until the beam and column separate completely (prestressing force will not generate compressive stress in the beam concrete). The CAA even generates negative contribution to load resistance when the vertical displacement exceeds about one beam depth.
4. Installing top-seat angle could improve the behavior by evoking flexural action and reducing the effective length of beam. On the other hand, the top-seat angle may lead to more severe damage in beam, especially in the beam end, resulting in less reparability of frame.
5. Higher effective prestress benefits the development of the resistance at small deformation. However, the higher effective prestress may reduce the deformation capacity of the strands, leading to the earlier strand fracture and lower ultimate load capacity.
6. Stronger boundary condition could improve the performance of the frame in terms of load resistance and deformation capacity. The failure of the specimens without overhanging beams was controlled by the large eccentric compression failure at the side columns. However, the failure of specimens with overhanging beams was controlled by the fracture of strands. Thus, the specimens have overhanging beam could fully use the material properties of the strands.

## 6. Acknowledgements

This research was supported by a research grant provided by the Natural Science Foundation of China (Nos. 51568004, 51778153, 51868004). Any opinions, findings and conclusions expressed in this paper are those of the writers and do not necessarily reflect the view of Natural Science Foundation of China.

## References


[1] Su YP, Tian Y, Song XS. Progressive collapse resistance of axially-restrained frame beams. ACI Structural Journal 2009; 106(5): 600-607.

[2] Sadek F, Main J, Lew H, Bao Y. Testing and analysis of steel and concrete beam-column assemblies under a column removal scenario. Journal of Structural Engineering 2011; 137(9): 881-892.

[3] Yu J, Tan KH. Experimental and numerical investigation on progressive collapse resistance of reinforced concrete beam column sub-assemblages. Engineering Structures 2013; 55: 90-106.

[4] Yu J, Tan KH. Special detailing techniques to improve structural resistance against progressive collapse. Journal of Structural Engineering 2014; 140(3): 04013077.

[5] Ren PQ, Li Y, Lu XZ, Guan H, Zhou YL. Experimental investigation of progressive collapse resistance of one-way reinforced concrete beam-slab substructures under a middle-column-removal scenario. Engineering Structures 2016; 118: 28-40.

[6] Lu XZ, Lin KQ, Li Y, Guan H, Ren PQ, Zhou YL. Experimental investigation of RC beam-slab substructures against progressive collapse subject to an edge-column-removal scenario. Engineering Structures 2017; 149: 91-103.

[7] Qian K, Li B, Ma JX. Load-carrying mechanism to resist progressive collapse of RC buildings. Journal of Structural Engineering 2015; 141(2): 04014107

[8] Qian K, Li B. Performance of Three-dimensional reinforced concrete beam-column substructures under loss of a corner column scenario. Journal of Structural Engineering 2013; 139(4): 584-594.

[9] Qian K, Li B. Dynamic performance of RC beam-column substructures under the scenario of the loss of a corner column—Experimental results. Engineering Structures 2012; 42: 154-167.

[10] Qian K, Li B. Slab effects on response of reinforced concrete substructures after loss of corner column. ACI structural Journal 2012; 109: 845-855.

[11] Qian K, Li B. Quantification of slab influences on the dynamic performance of RC frames against progressive collapse. J. Perform. Constr. Facil 2015; 29(1): 04014029.

[12] Shan SD, Li S, Xu SY, Xie LL. Experimental study on the progressive collapse performance of RC frames with infill walls. Engineering Structures 2016; 111: 80-92.

[13] Peng ZH, Orton SL, Liu JR, Tian Y. Experimental study of dynamic progressive collapse in flat-plate buildings subjected to exterior column removal. Journal of Structural Engineering 2017; 143(9): 04017125.

[14] Peng ZH, Orton SL, Liu JR, Tian Y. Experimental study of dynamic progressive collapse in flat-plate buildings subjected to interior column removal. Journal of Structural Engineering 2018; 144(8): 04018094.

[15] Ma F, Gilbert B, Guan H, Xue HZ, Lu XZ, Li Y. Experimental study on the progressive collapse behaviour of RC flat plate substructures subjected to corner column removal scenarios. Engineering Structures 2019; 180: 728-741.

[16] Qian K, Weng YH, Li B. Improving behavior of reinforced concrete frames to resist progressive collapse through steel bracings. Journal of Structural Engineering 2019; 145(2): 04018248.

[17] Sasani M, Bazan M, Sagiroglu S. Experimental and analytical progressive collapse evaluation of actual reinforced concrete structure. ACI Structural Journal 2007; 104(6): 731-9.

[18] Sasani M, Sagiroglu S. Progressive collapse resistance of Hotel San Diego. Journal of Structural Engineering 2008; 134(3): 478-88.

[19] Sasani M. Response of a reinforced concrete infilled-frame structure to removal of two adjacent columns. Engineering Structures 2008; 30: 2478-91.

[20] Sasani M, Sagiroglu S. Gravity load redistribution and progressive collapse resistance of 20-story reinforced concrete structure following loss of interior column. ACI Structural Journal 2010; 107(6): 636-44.

[21] Sasani M, Kazemi A, Sagiroglu S, Forest S. Progressive collapse resistance of an actual 11-story structure subjected to severe initial damage. Journal of Structural Engineering 2011; 137(9): 893-902.

[22] Nimse RB, Joshi DD, Oatel PV. Behavior of wet precast beam column connections under progressive collapse scenario: an experimental study. International Journal of Advanced Structural Engineering 2014; 6: 149-159.

[23] Kang SB, Tan KH. Behaviour of precast concrete beam-column sub-assemblages subject to column removal. Engineering Structures 2015; 93: 85-96.

[24] Kang SB, Tan KH. Robustness assessment of exterior precast concrete frames under column removal scenarios. Journal of Structural Engineering 2016; 142(12): 04016131.

[25] Keyvani L. Progressive collapse resistance of reinforced and post-tensioned flat plate structures. PhD Dissertation, The Department of Civil and Environmental Engineering, Northeastern University; 2015.

[26] Keyvani L, Sasani M. Analytical and experimental evaluation of progressive collapse resistance of a flat-slab posttensioned parking garage. Journal of Structural Engineering 2015; 141(11): 04015030.

[27] Qian K, Li B. Investigation into resilience of precast concrete floors against progressive collapse. ACI Structural Journal 2019; 116(2): 171-182.

[28] Al-Salloum YA, Alrubaidi MA, Elsanadedy HM, Almusallam TH, Iqbal RA. Strengthening of precast RC beam-column connections for progressive collapse mitigation using bolted steel plates. Engineering Structures 2018; 161: 146-160.

[29] Quiel SE, Naito CJ, Fallon CT. A non-emulative moment connection for progressive collapse resistance in precast concrete building frames. Engineering Structures 2019; 179: 174-188.
[30] Qian K, Li B. Performance of precast concrete substructures with dry connections to resist progressive collapse. Journal of Performance of Constructed Facilities 2018; 32(2): 04018005.
[31] Priestley MJN, MacRae G. Seismic tests of precast beam-to-column joint subassemblages with unbonded strands. PCI J 1996; 41(1): 64-81.
[32] Cheok G, Lew H. Model precast concrete beam-to-column joints subject to cyclic loading. PCI J 1993; 38(4): 80-92.
[33] Stone WC, Cheok GS, Stanton JF. Performance of hybrid moment-resisting precast beam-column concrete connection subjected to cyclic loading. ACI Structural Journal 1995; 92(2): 229-49.
[34] Stanton J, Stone WC, and Cheok GS. A Hybrid Reinforced Precast Frame for Seismic Regions. PCI Journal 1997, 42(2): 20-32.
[35] Rodgers GW, Solberg KM, Chase JG, Mander JB, Bradley BA, Dhakal RP, Li L. Performance of a damage-protected beam-column subassembly utilizing external HF2V energy dissipation devices. Earthquake Engineering and Structural Dynamics 2008; 37(13): 1549–64.
[36] Rodgers GW, Solberg KM, Mander JB, Chase JG, Bradley BA, Dhakal RP. Highforce-to-volume seismic dissipaters embedded in a jointed precast concrete frame. Journal of Structural Engineering 2012; 138(3): 375–86.
[37] Song LL, Guo T, Chen C. Experimental and numerical study of a self-centering prestressed concrete moment resisting frame connection with bolted web friction devices. Earthquake Engineering and Structural Dynamics 2014; 43(4): 529–45.
[38] Song LL, Guo T, Gu Y, Cao ZL. Experimental study of a self-centering prestressed concrete frame subassembly. Engineering Structures 2015; 88: 176-188.
[39] ACI Committee 318, Building Code Requirements for Structural Concrete (ACI 318-14) and Commentary (318R-14). American Concrete Institute, Farmington Hills, MI, 433 pp; 2014.
[40] Cheok GS and Lew HS. Performance of precast concrete beam-to-column connections subject to cyclic loading. PCI Journal 1991, 36(3): pp. 56-67.
[41] Izzuddin B, Vlassis A, Elghazouli A, Nethercot D. Progressive collapse of multi-storey buildings due to sudden column loss-part I: simplified assessment framework. Engineering Structures 2008; 30: 1308-1318.

**Figure caption list**

**Fig. 1.** Bending moment diagram of a frame: (a) before removal of column; (b) after removal of column

**Fig. 2.** Tested connections: (a) unbonded post-tensioning connection; (b) hybrid connection; (c) bolted top-seat angle connection

**Fig. 3.** Details of test specimens: (a) TSUPI; (b) UPE; (c) cross sections

**Fig. 4.** Stress-strain constitutive curves: (a) rebar; (b) post-tensioning strands

**Fig. 5.** Test setup and instrumentation: (a) photo; (b) elevation view

**Fig. 6.** Vertical load-displacement curves

**Fig. 7.** Failure mode of TSE

**Fig. 8.** Failure mode of TSI

**Fig. 9.** Failure mode of UPE-0.4

**Fig. 10.** Failure mode of UPI-0.4

**Fig. 11.** Failure mode of UPI-0.65

**Fig. 12.** Failure mode of TSUPE-0.4

**Fig. 13.** Failure mode of TSUPI-0.4

**Fig. 14.** Failure mode of TSUPI-0.65

**Fig. 15.** Comparison of the horizontal reaction force versus MJD curves

**Fig. 16.** Contribution of horizontal reaction force from each constraint: (a) UPI-0.4; (b) UPE-0.4

**Fig. 17.** Overall deflection of double-bay beam: (a) UPI-0.65; (b) TSUPI-0.65

**Fig. 18.** Horizontal deformation in side column: (a) TSUPE-0.4; (b) TSUPI-0.4

**Fig. 19.** Strain distribution in beam longitudinal reinforcement of UPE-0.4: (a) bottom rebar; (b) top rebar

**Fig. 20.** Strain distribution in beam longitudinal reinforcement of UPI-0.4: (a) bottom rebar; (b) top rebar

**Fig. 21.** Strain distribution in beam longitudinal reinforcement of TSUPI-0.4: (a) bottom rebar; (b) top rebar

**Fig. 22.** Total prestressing forces-displacement relationship

**Fig. 23.** Discussion of each design variable: (a) TSUPI-0.4; (b) TSUPE-0.4; (c) TSUPI-0.65

**Fig. 24.** Dynamic resistance of tested specimens

**Fig. 25.** Load resisting mechanism of RC structure: (a) compressive arch action; (b) tensile catenary action

**Fig. 26.** Load resisting mechanisms of specimens with unbonded post-tensioning connection: (a) small deformation; (b) MJD beyond one beam depth

**Fig. 27.** Resistance decomposition of specimen UPI-0.65

**Fig. 28** Load resisting mechanism of specimens with hybrid connection

**Table 1**. Relationship between prototype frames and corresponding test specimens

| Test ID | Prototype frame | | | Test specimen | | |
|---|---|---|---|---|---|---|
| | Column (mm × mm) | Beam (mm × mm) | Diameter of strands (mm) | Column (mm × mm) | Beam (mm × mm) | Diameter of strands (mm) |
| TSE | 500×500 | 500×300 | N/A | 250×250 | 250×150 | N/A |
| TSI | 500×500 | 500×300 | N/A | 250×250 | 250×150 | N/A |
| UPE-0.4 | 500×500 | 500×300 | 4×17.8 | 250×250 | 250×150 | 2×12.7 |
| UPE-0.65 | 500×500 | 500×300 | 4×17.8 | 250×250 | 250×150 | 2×12.7 |
| UPI-0.4 | 500×500 | 500×300 | 4×17.8 | 250×250 | 250×150 | 2×12.7 |
| UPI-0.65 | 500×500 | 500×300 | 4×17.8 | 250×250 | 250×150 | 2×12.7 |
| TSUPI-0.4 | 500×500 | 500×300 | 4×17.8 | 250×250 | 250×150 | 2×12.7 |
| TSUPI-0.65 | 500×500 | 500×300 | 4×17.8 | 250×250 | 250×150 | 2×12.7 |

**Table 2.** Specimens properties

| Test ID | Span/depth ratio | Axial compression ratio | Top (Bottom) beam rebar ratio ρ | Column rebar ratio ρ | Effective prestress | Top-seat angle | Overhanging beam |
|---|---|---|---|---|---|---|---|
| TSE | 12 | 0.2 | 0.6% (0.6%) | 1.4% | N/A | L160×12 | N/A |
| TSI | 12 | 0.2 | 0.6% (0.6%) | 1.4% | N/A | L160×12 | Yes |
| UPE-0.4 | 12 | 0.2 | 0.6% (0.6%) | 1.4% | $0.4f_{pu}$ | N/A | N/A |
| UPI-0.4 | 12 | 0.2 | 0.6% (0.6%) | 1.4% | $0.4f_{pu}$ | N/A | Yes |
| UPI-0.65 | 12 | 0.2 | 0.6% (0.6%) | 1.4% | $0.65f_{pu}$ | N/A | Yes |
| TSUPE-0.4 | 12 | 0.2 | 0.6% (0.6%) | 1.4% | $0.4f_{pu}$ | L160×12 | N/A |
| TSUPI-0.4 | 12 | 0.2 | 0.6% (0.6%) | 1.4% | $0.4f_{pu}$ | L160×12 | Yes |
| TSUPI-0.65 | 12 | 0.2 | 0.6% (0.6%) | 1.4% | $0.65f_{pu}$ | L160×12 | Yes |

Note: $f_{pu}$ is the nominal ultimate strength of the post-tensioning strands (1860 MPa); rebar ratio is determined using equation $\rho = A_s/bd_0$, in which $A_s$, b and $d_0$ represent the area of rebar, width and the effective depth of beam cross sections, respectively.

**Table 3.** Material properties

| Item | Nominal diameter (mm) | Yield strength (MPa) | Ultimate strength (MPa) | Elastic modulus (MPa) | Elongation (%) |
|---|---|---|---|---|---|
| Transverse reinforcements R6 | 6 | 368 | 485 | 162,000 | 20.1 |
| Longitudinal reinforcements T12 | 12 | 462 | 596 | 171,000 | 14.7 |
| Longitudinal reinforcements T16 | 16 | 466 | 604 | 182,000 | 17.0 |
| Posttensioning strands | 12.7 | 1,649 | 1,970 | 213,000 | 6.3 |

**Table 4.** Summary of test results

| Specimen identifier | Critical displacement (mm) | | Critical load (kN) | | Maximum prestressing force (kN) | Maximum horizontal compressive/tensile force (kN) |
|---|---|---|---|---|---|---|
| | First peak load | Ultimate load | First peak load | Ultimate load | | |
| TSE | 70 | 70 | 12 | 12 | N/A | -37/18 |
| TSI | 100 | 100 | 12 | 12 | N/A | -44/3 |
| UPE-0.4 | 45 | 540 | 30 | 73 | 269 | -66/139 |
| UPI-0.4 | 29 | 652 | 35 | 151 | 324 | -96/323 |
| UPI-0.65 | 39 | 542 | 44 | 131 | 326 | -84/321 |
| TSUPE-0.4 | 100 | 522 | 49 | 83 | 277 | -50/146 |
| TSUPI-0.4 | 95 | 600 | 51 | 181 | 364 | -93/380 |
| TSUPI-0.65 | 76 | 600 | 64 | 178 | 368 | -113/364 |

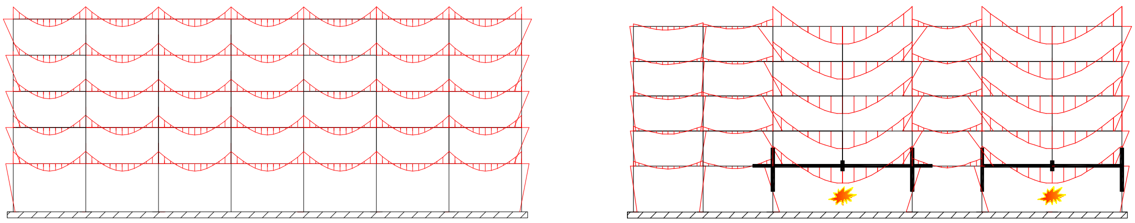

(a) (b)

**Fig. 1.** Bending moment diagram of a frame: (a) before removal of column; (b) after removal of column

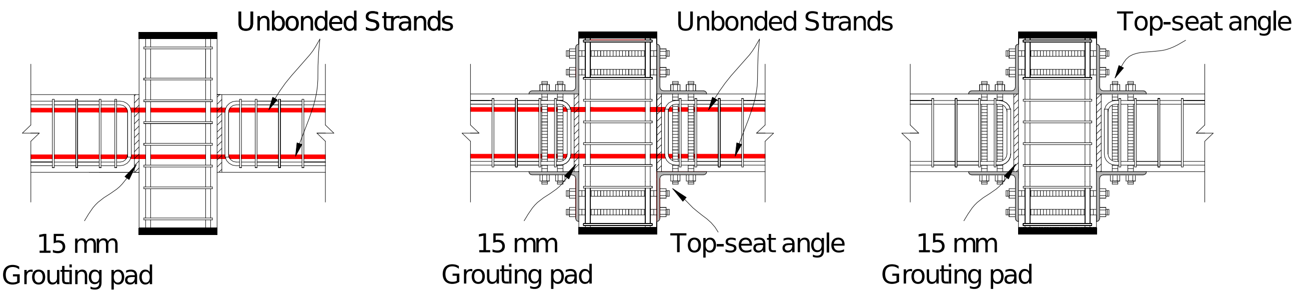


(a) (b) (c)

**Fig. 2.** Test connections: (a) unbonded post-tensioning connection; (b) hybrid connection; (c) bolted top-seat angle connection

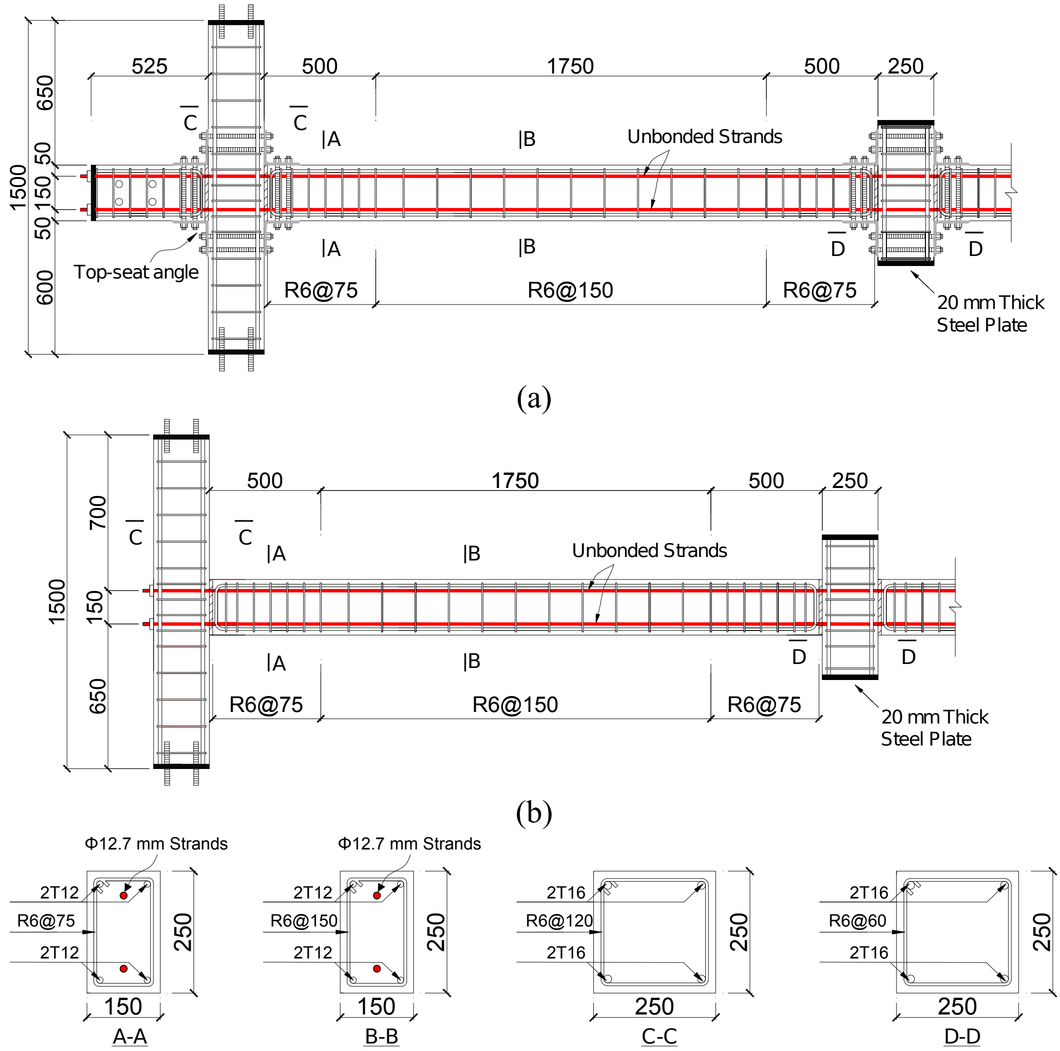


**Fig. 3.** Details of test specimens: (a) TSUPI; (b) UPE; (c) cross sections

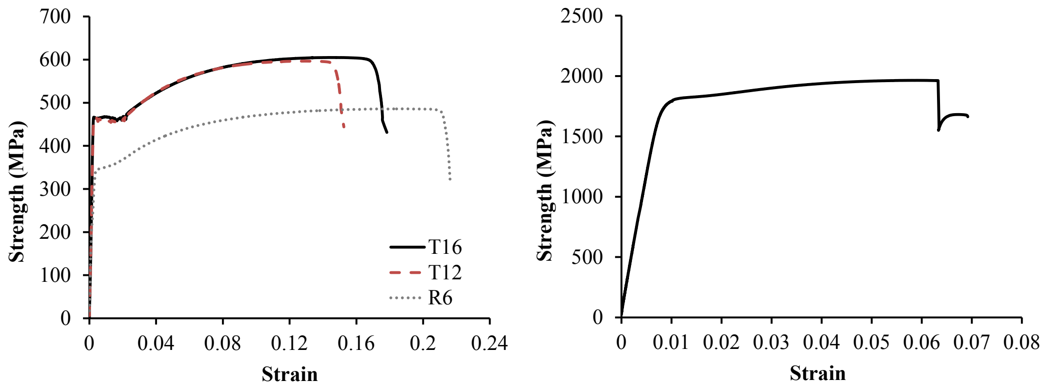


(a) (b)

**Fig. 4.** Stress-strain constitutive curves: (a) rebar; (b) post-tensioning strands

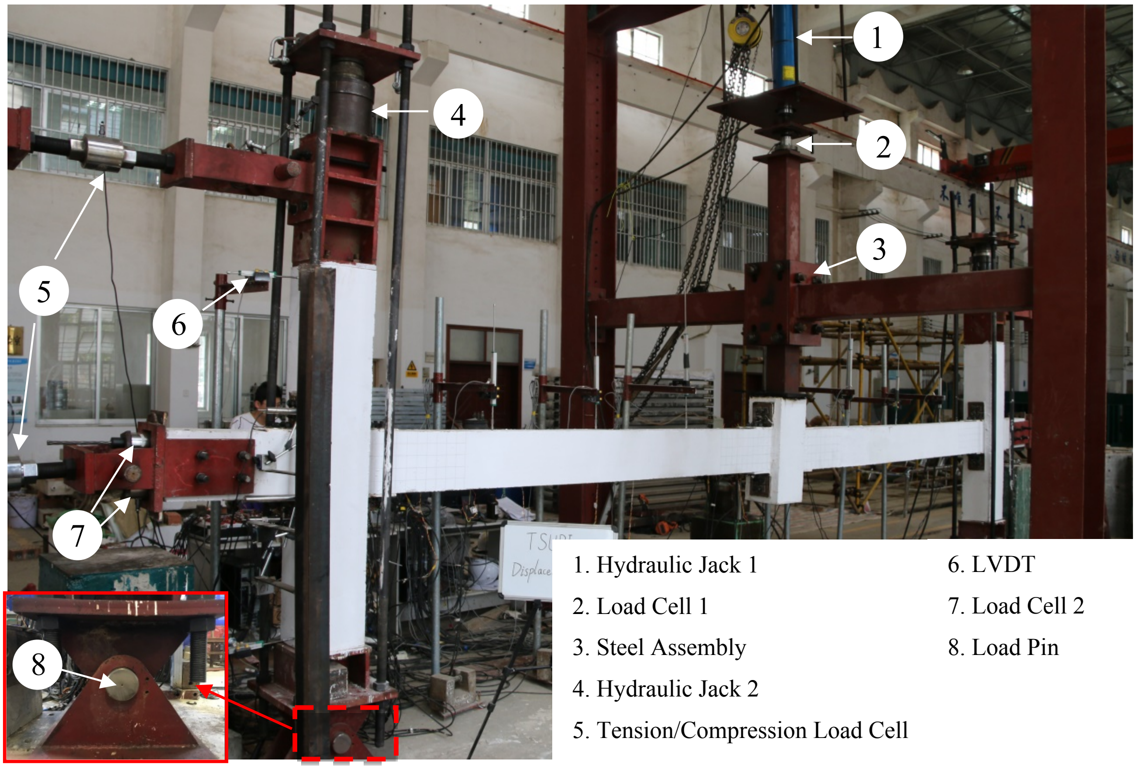


(a)

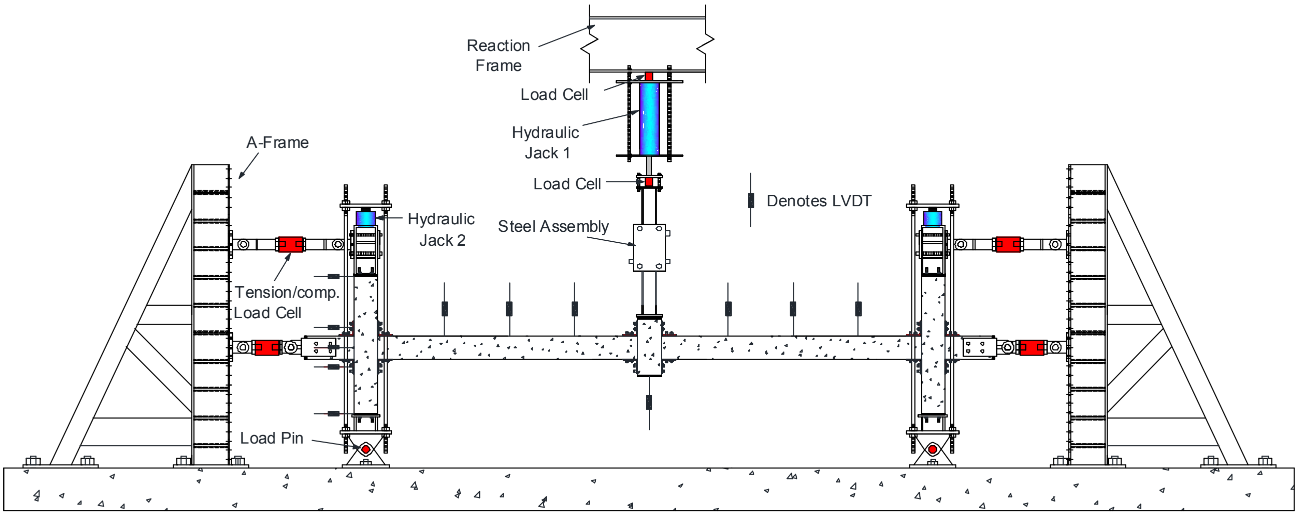


(b)

**Fig. 5.** Test setup and instrumentation: (a) photo; (b) elevation view

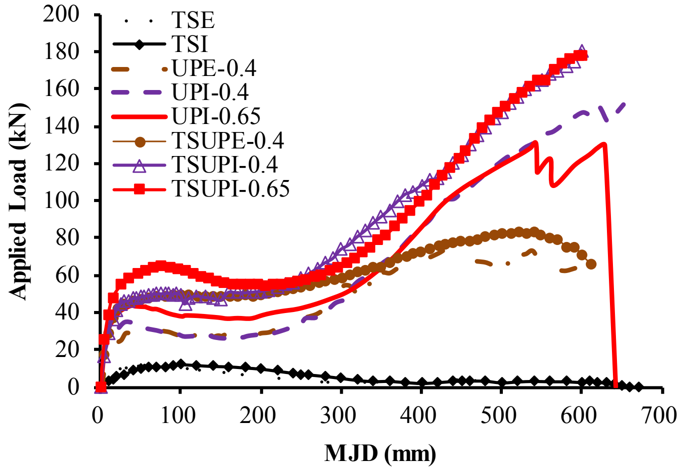


**Fig. 6.** Vertical load-displacement curves

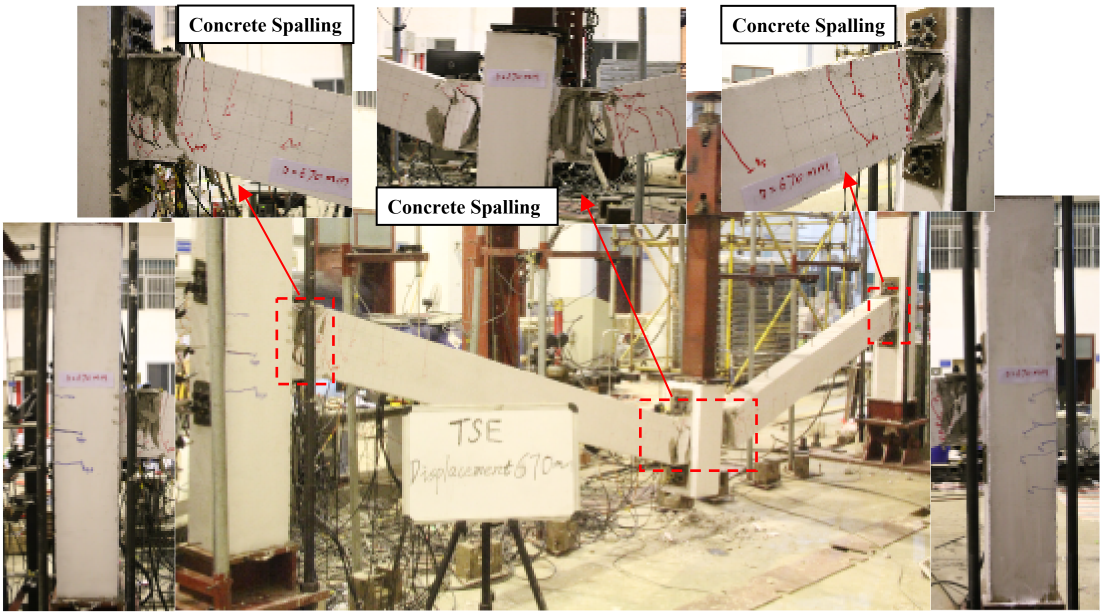


**Fig. 7.** Failure mode of TSE

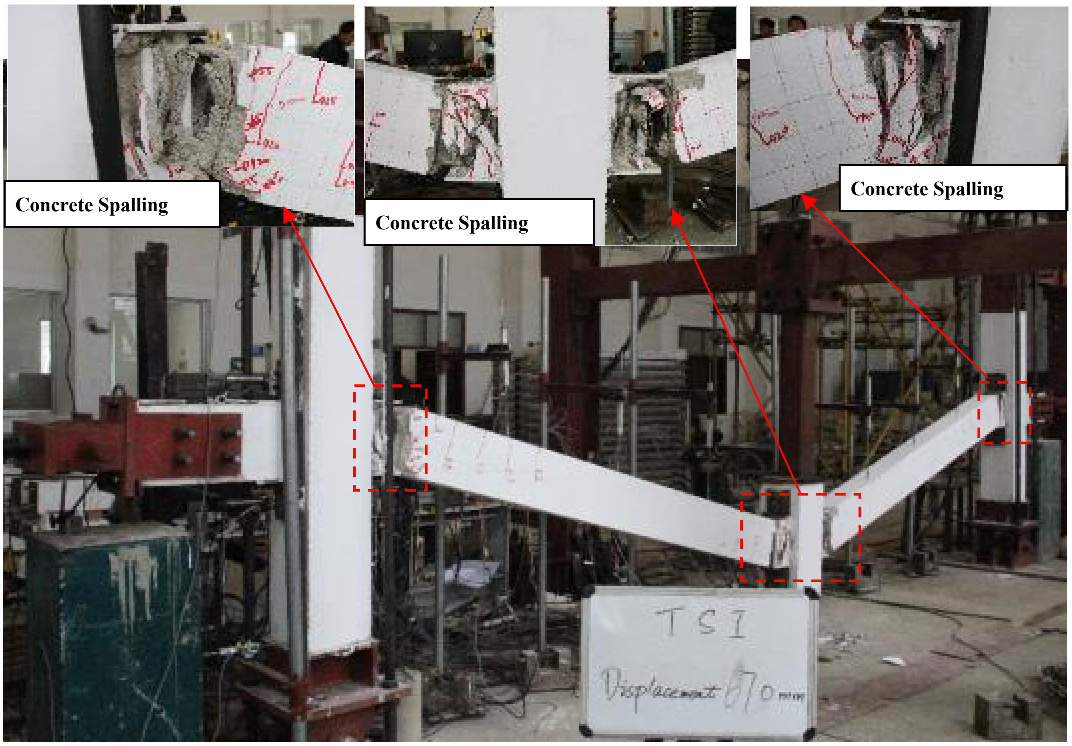


**Fig. 8.** Failure mode of TSI

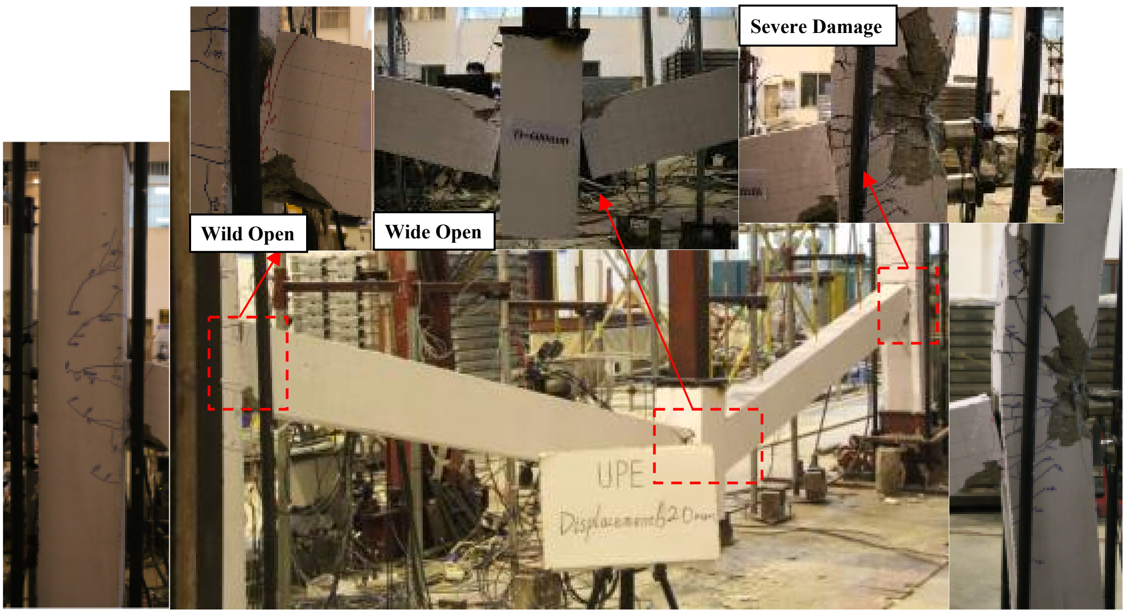


**Fig. 9.** Failure mode of UPE-0.4

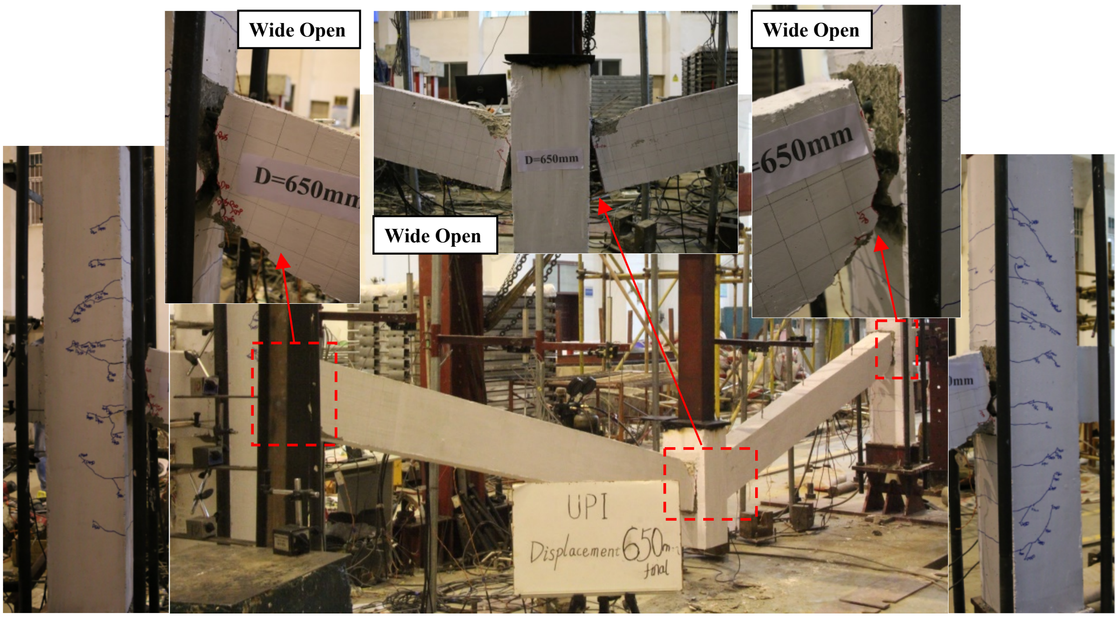


**Fig. 10.** Failure mode of UPI-0.4

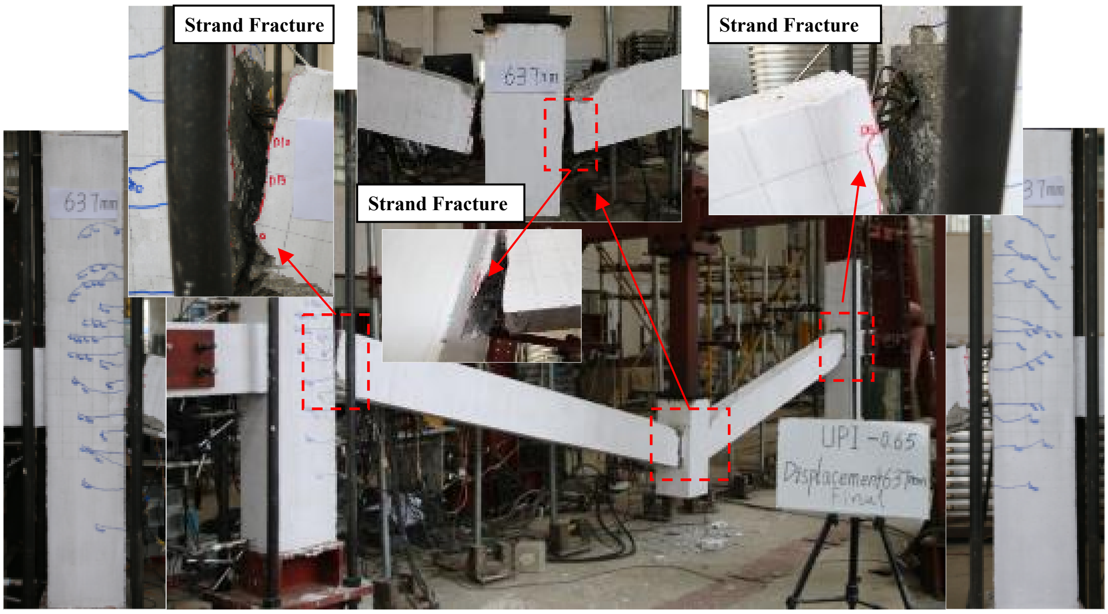


**Fig. 11.** Failure mode of UPI-0.65

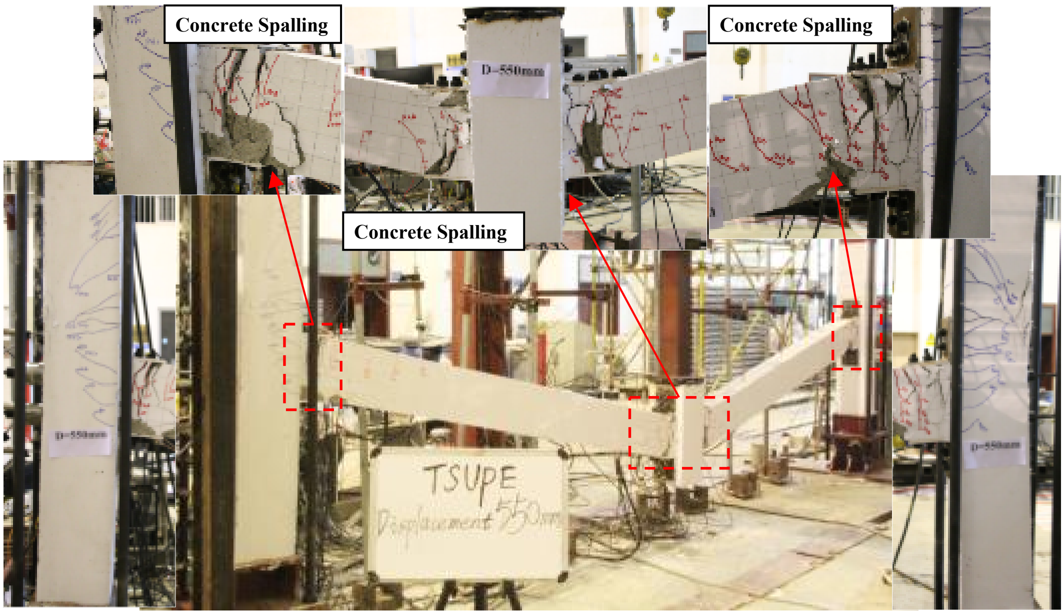


**Fig. 12.** Failure mode of TSUPE-0.4

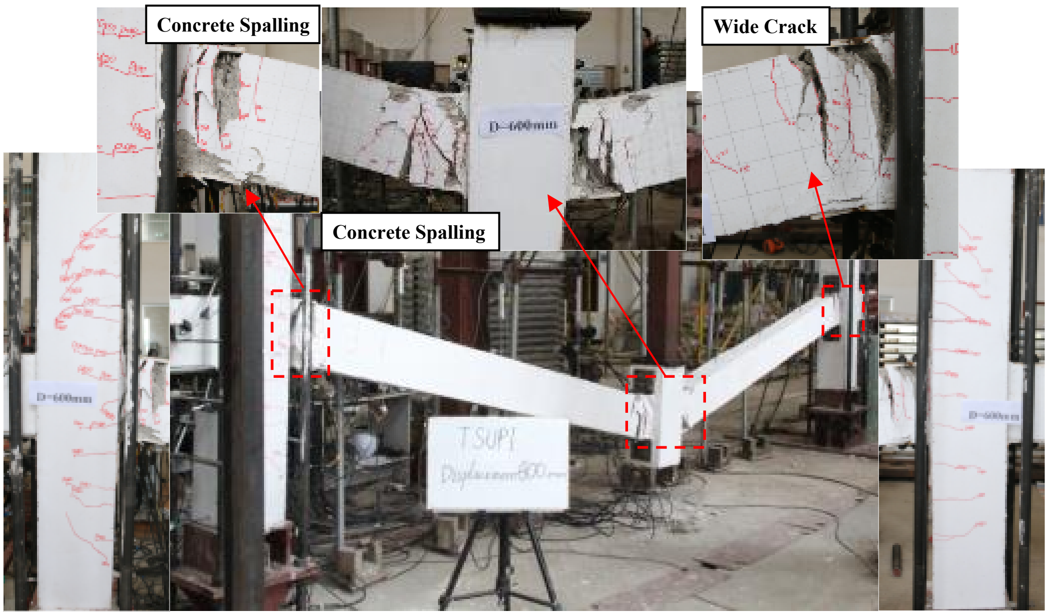


**Fig. 13.** Failure mode of TSUPI-0.4

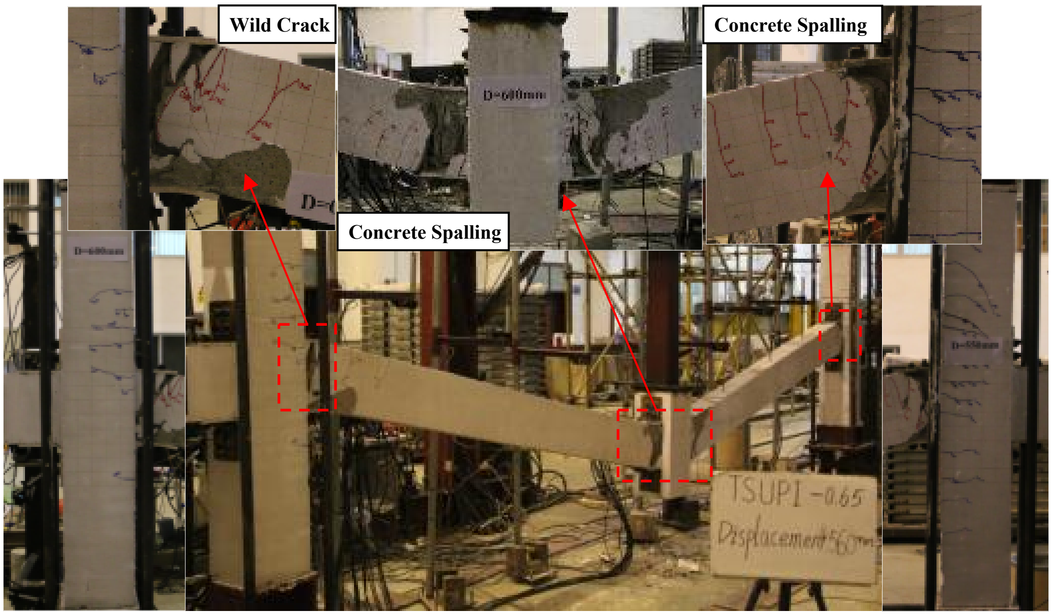


**Fig. 14.** Failure mode of TSUPI-0.65

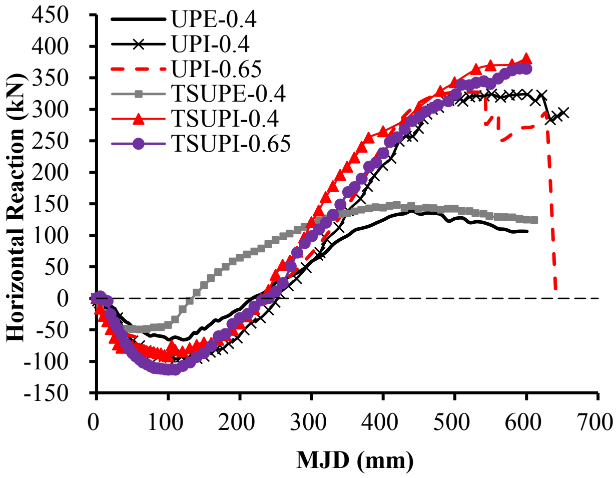


**Fig. 15.** Comparison of the horizontal reaction force versus MJD curves

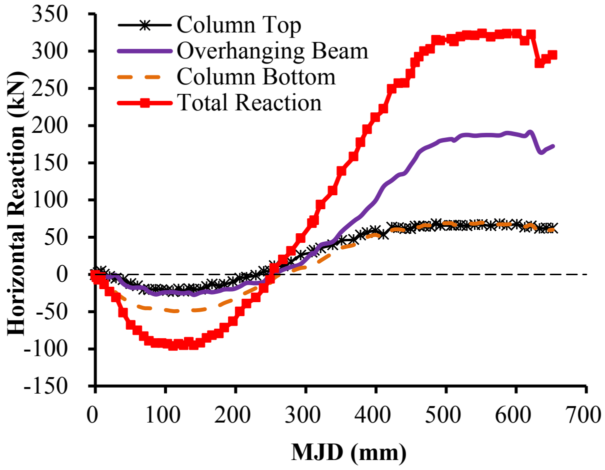


(a)

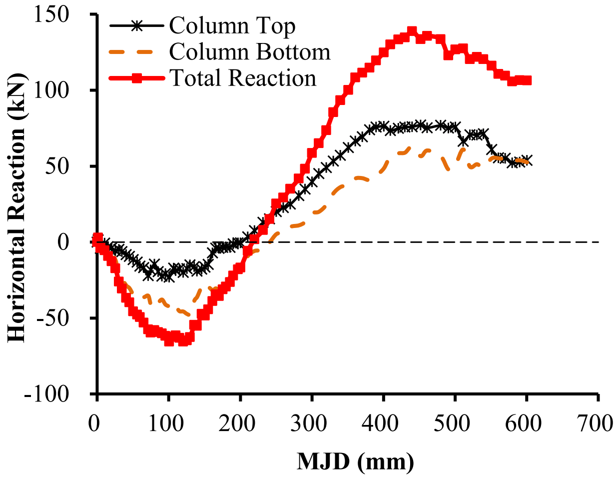


(b)

**Fig. 16.** Contribution of horizontal reaction force from each constraint: (a) UPI-0.4; (b) UPE-0.4

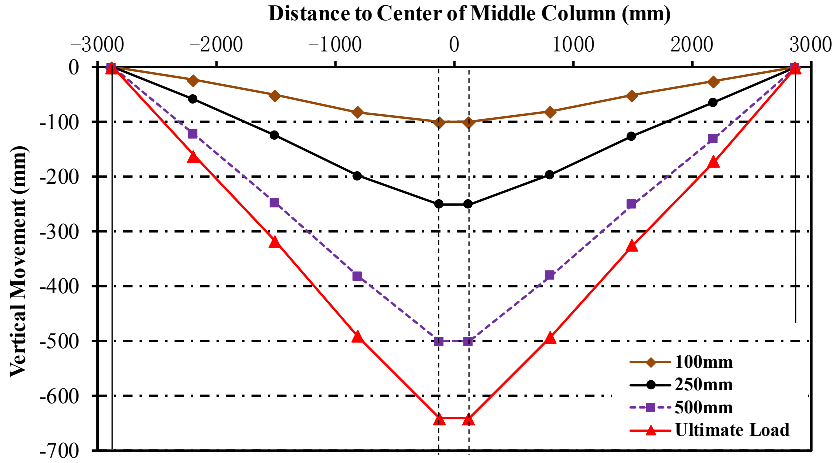


(a) UPI-0.65

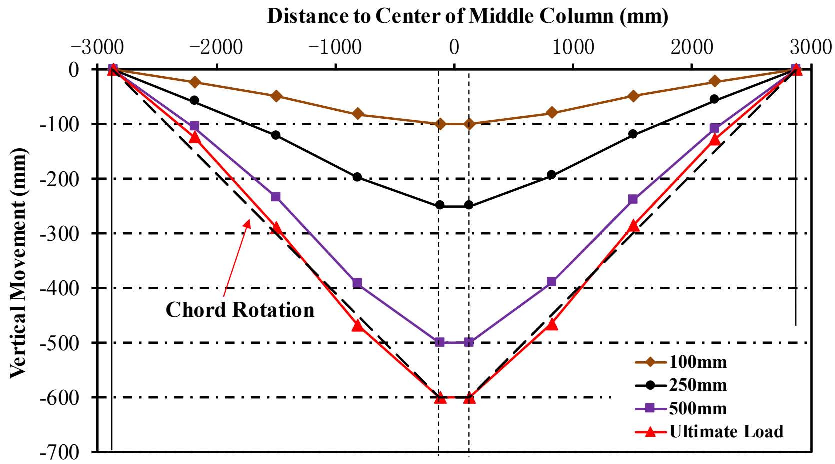


(b) TSUPI-0.65

**Fig. 17.** Overall deflection of double-bay beam: (a) UPI-0.65; (b) TSUPI-0.65

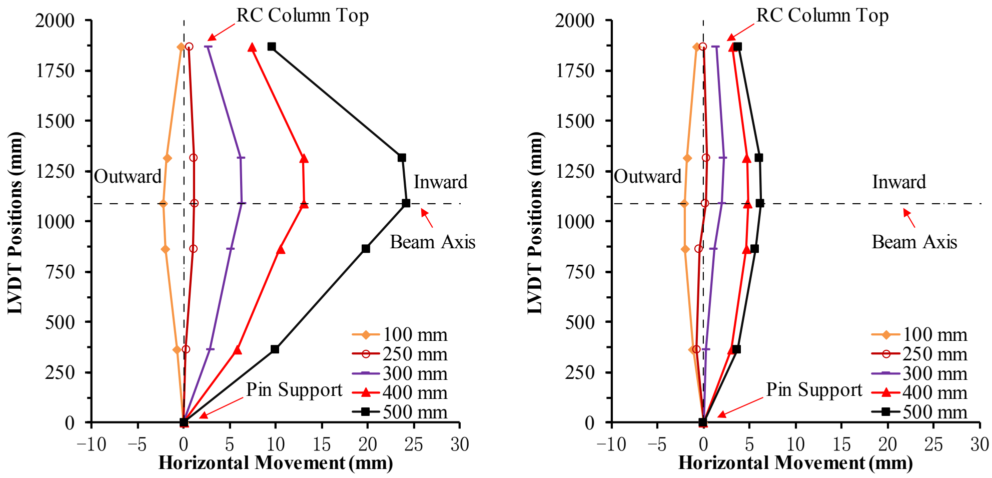


(a) (b)

**Fig. 18.** Horizontal deformation in side column: (a) TSUPE-0.4; (b) TSUPI-0.4

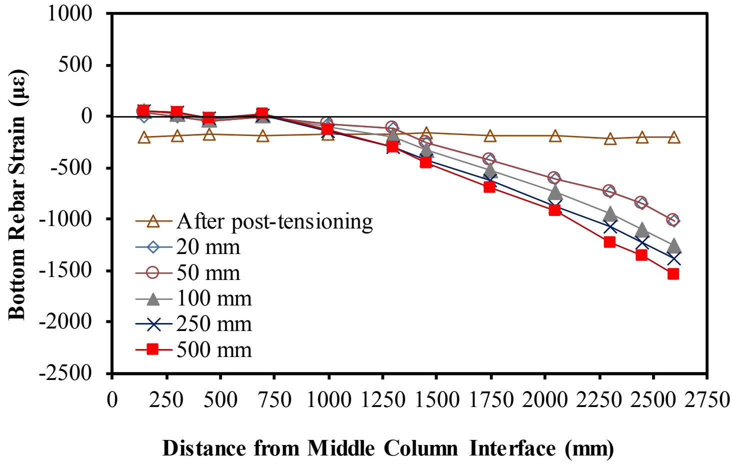


(a)

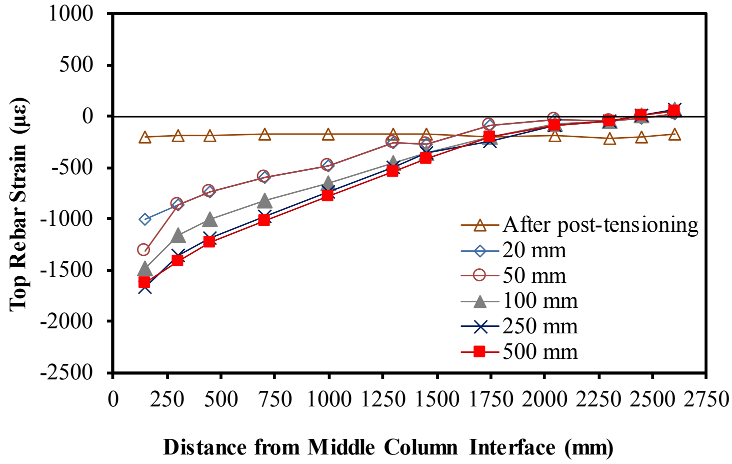


(b)

**Fig. 19.** Strain distribution in beam longitudinal reinforcement of UPE-0.4: (a) bottom rebar; (b) top rebar

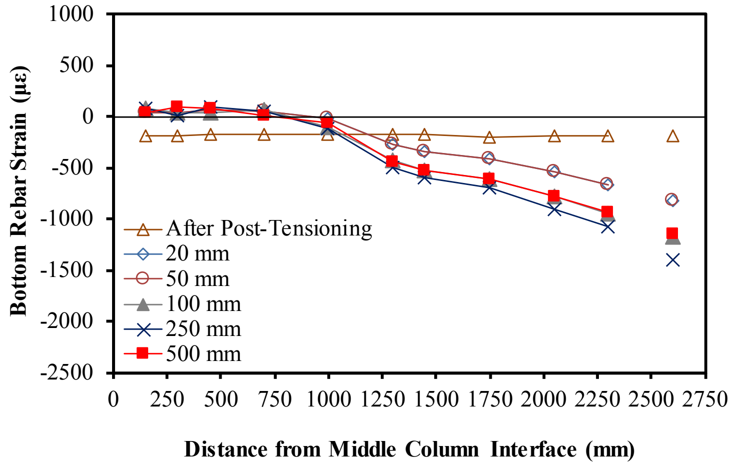


(a)

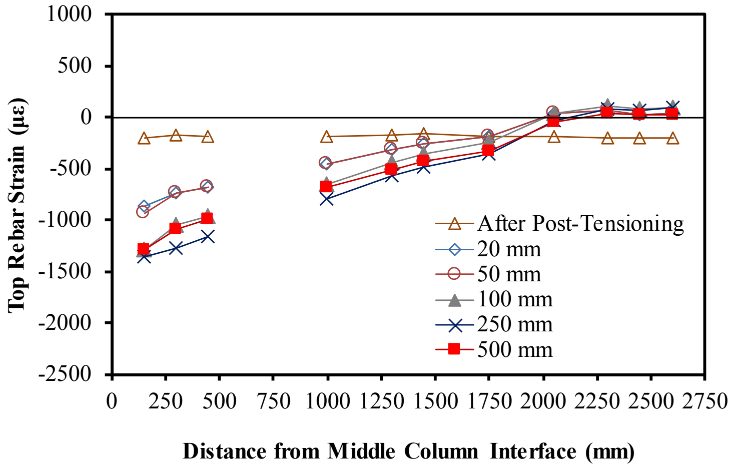


(b)

**Fig. 20.** Strain distribution in beam longitudinal reinforcement of UPI-0.4: (a) bottom rebar; (b) top rebar

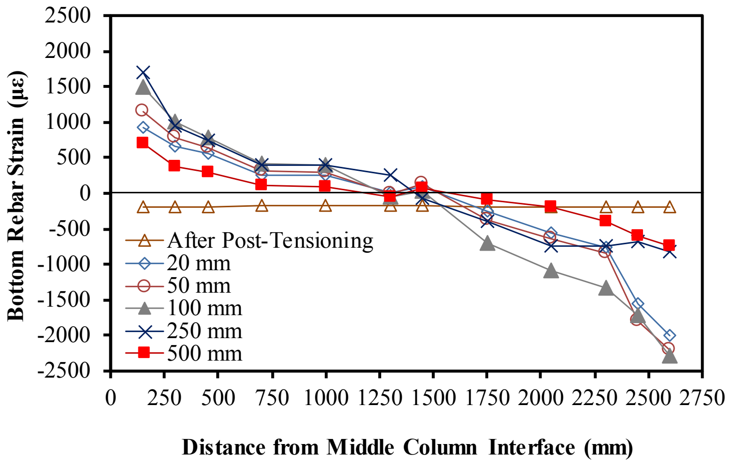


(a)

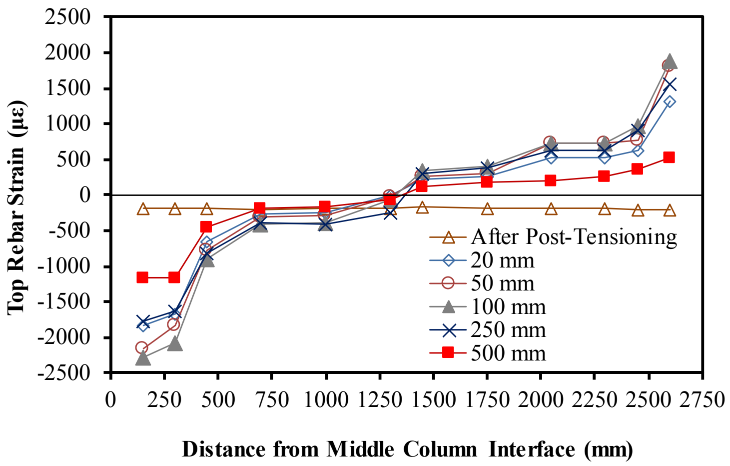


(b)

**Fig. 21.** Strain distribution in beam longitudinal reinforcement of TSUPI-0.4: (a) bottom rebar; (b) top rebar

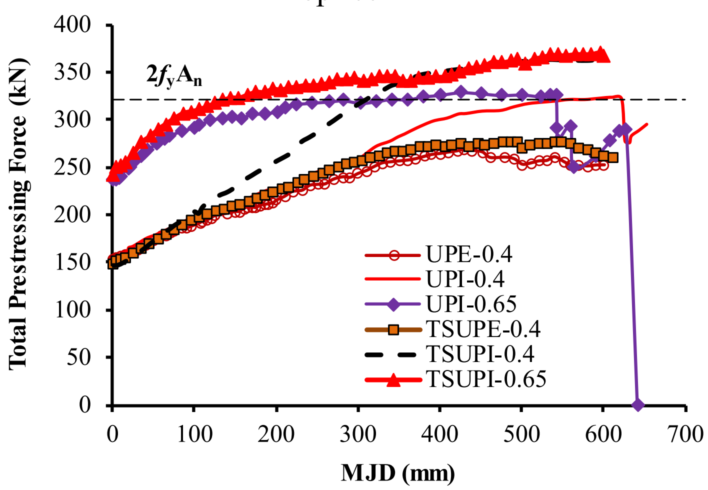


**Fig. 22.** Total prestressing forces-displacement relationship

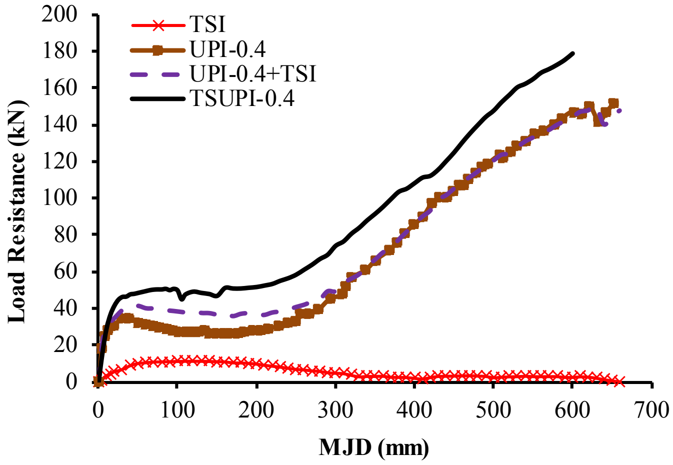


(a)

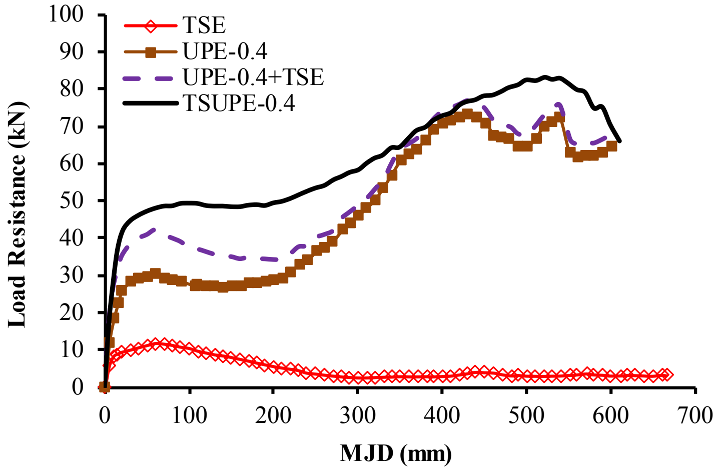


(b)

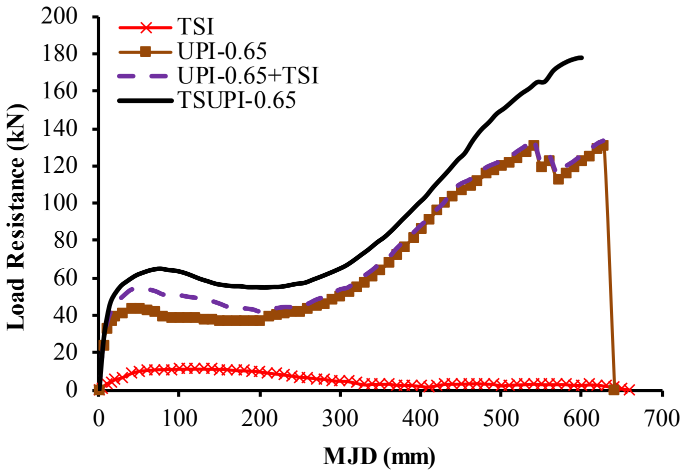


(c)

**Fig. 23.** Discussion of each design variable: (a) TSUPI-0.4; (b) TSUPE-0.4; (c) TSUPI-0.65

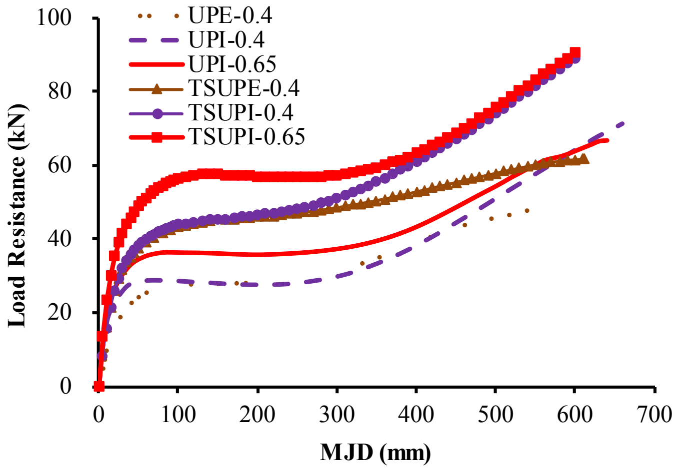


**Fig. 24.** Dynamic resistance of tested specimens

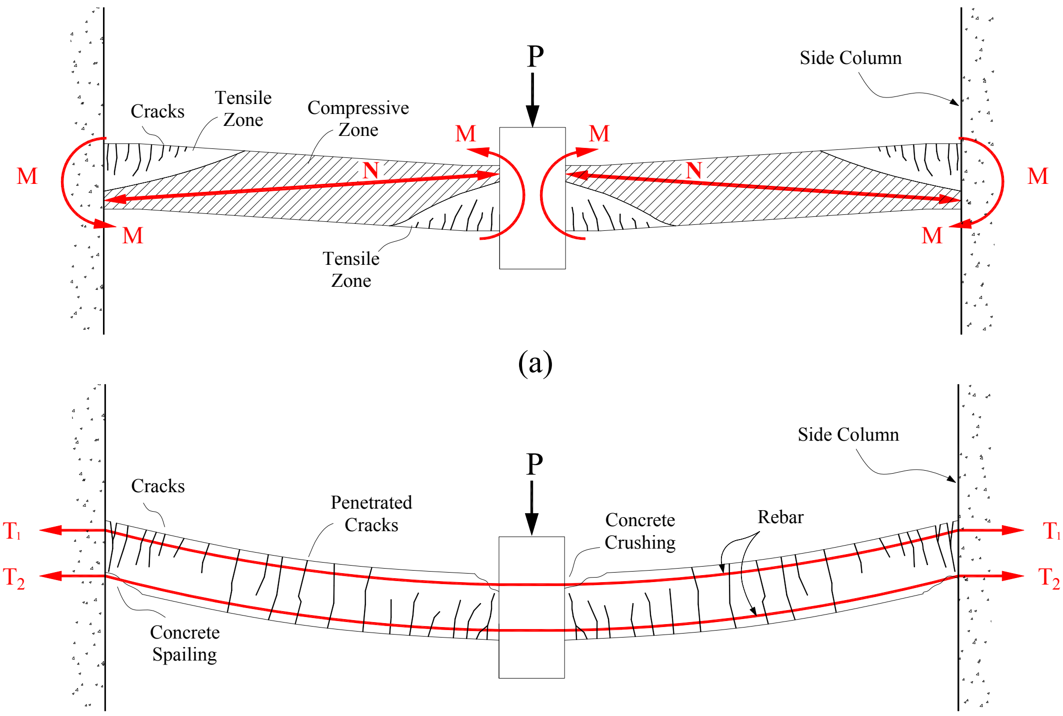


(a)

(b)

**Fig. 25.** Load resisting mechanism of RC structure: (a) compressive arch action; (b) tensile catenary action

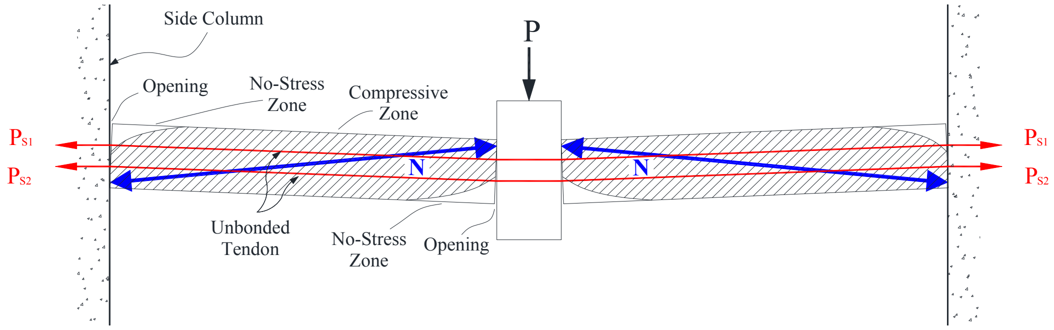


(a)

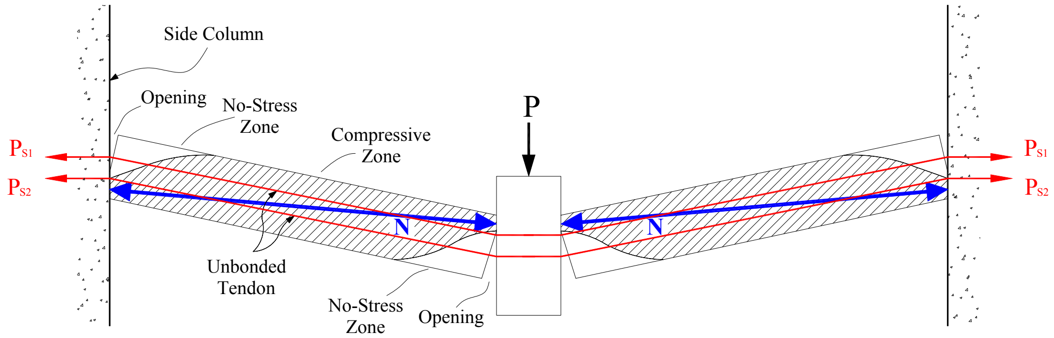


(b)

**Fig. 26.** Load resisting mechanisms of specimens with unbonded post-tensioning connection: (a) small deformation; (b) MJD beyond one beam depth

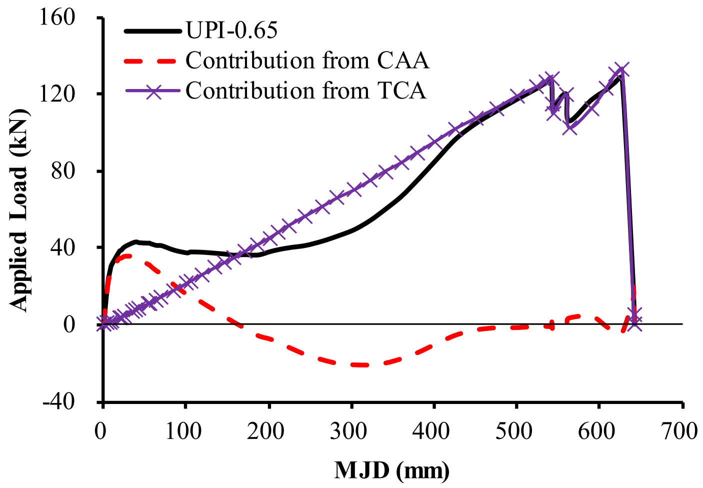


**Fig. 27.** Resistance decomposition of specimen UPI-0.65

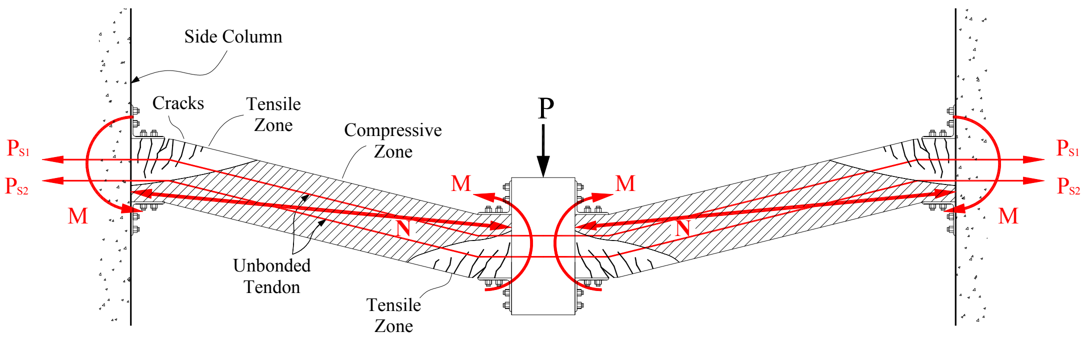


**Fig. 28.** Load resisting mechanism of specimens with hybrid connection